12-1-2008

Rainbows in the Grass. I. External Reflection Rainbows from Pendant Droplets

James A. Lock
Cleveland State University, j.lock@csuohio.edu

Charles L. Adler

Richard W. Fleet

Original Citation

Lock, James A., Charles L. Adler, and Richard W. Fleet. "Rainbows in the Grass. I. External Reflection Rainbows from Pendant Droplets." *Applied Optics* 47 (2008): H203-H213.

Repository Citation

Lock, James A.; Adler, Charles L.; and Fleet, Richard W., "Rainbows in the Grass. I. External Reflection Rainbows from Pendant Droplets" (2008). *Physics Faculty Publications*. 33.
https://engagedscholarship.csuohio.edu/sciphysics_facpub/33

Rainbows in the grass. I. External-reflection rainbows from pendant droplets

James A. Lock,[1] Charles L. Adler,[2,*] and Richard W. Fleet[3]

[1]Department of Physics, Cleveland State University, Cleveland, Ohio 44115, USA

[2]Department of Physics, St. Mary's College of Maryland, St. Mary's City, Maryland 20618, USA

[3]Newbury Astronomical Society, Newbury, Berkshire RG14 7TZ, UK

*Corresponding author: cladler@smcm.edu

In the mid-morning on a sunny day one can sometimes see glare spots associated with uncolored "rainbow" (i.e., fold) caustics due to the sunlight reflected from the surface of dew or guttation drops. We show that these dewdrop reflection rainbows are due to places on the droplet (i.e., from an "inflection circle") where its Gaussian curvature becomes zero. We work out the theory of such caustics with horizontally incident light and present a comparison of the theory to measurements made in the laboratory.   © 2008 Optical Society of America

OCIS codes: 010.7340, 290.0290.

1. Introduction

Since the 1970s it has been recognized that optical caustics are a generic feature of light scattering by objects of arbitrary shape; to quote Stavroudis, "the caustic is one of the few things in geometrical optics that has any physical reality… rays… are not realizable; they are just convenient symbols on which to hang our ideas" [1]. The atmospheric rainbow is easily the most widely recognized example of a caustic (the fold caustic) because it is one of the most frequently occurring and most beautiful atmospheric optical phenomena. However, the most visible feature of the rainbow—its coloration—is the least pertinent to its study as an example of an optical caustic; the colors are due to the dispersion of light, which is not a central feature of the caustic. The **brightness** of light in the vicinity of the rainbow, its true key feature, is due to the presence of an extremum in the scattering angle as a function of the impact parameter of a light ray entering a water droplet, which is then refracted and reflected to a dis-

tant observer's eye [2]. Or, in wave theory, the fold caustic is due to truncation at the cubic term in the expansion of the phase of the wave in the near field [3].

In a recent publication, one of the authors used the rainbow caustic associated with the refraction of light by a draining vertical fluid layer to determine the surface tension of the liquid [4]. The caustic was caused by the shape of the fluid surface; that is, a point of inflection where the radius of curvature becomes infinite exists owing to the balance of viscous forces against the surface tension of the liquid [5]. In this case, the refraction of light through the surface to produce the caustic is not essential, as reflection of light from the surface would produce a similar fold caustic, as the phase of the light wave is proportional to the local surface shape. (This is in contrast to the atmospheric rainbow, where the phase is determined by refraction into the droplet, one or more internal reflections, and refraction out of the droplet [2,3].) Thus, reflection or refraction from any surface in which a local parameterization of the surface shape has a point where the second derivative vanishes can be expected to lead to a rainbow caustic in the far field for light reflected or refracted by the surface.

An example of such a surface is a pendant droplet, that is, a droplet hanging from some support above it. As discussed below, the shape of the droplet is determined by the balancing of the forces of gravity and the surface tension of the fluid; "necking" of the droplet near the line of attachment to the support leads to an "inflection circle" (defined more rigorously below) along which the Gaussian curvature vanishes. If we shine a light beam onto the droplet near the inflection circle, the reflection of light from the droplet will have a caustic in the far field; that is, projection of the reflection onto a screen in the far field will lead to a fold caustic. An observer placing his or her head to intercept the rays reflected from this spot will see a glare spot due to the caustic, and out-of-focus imaging will show a set of unequally spaced Airy fringes due to the caustic.

Figures 1 and 2 show an example of this in photographs taken in the garden of one of the authors. Figure 1 shows a close-up image of a pendant drop on a blade of grass, with a glare spot clearly visible near the point of attachment of the droplet to the grass blade. Figure 2 is an out-of-focus image showing the resultant Airy fringes of the caustic. In the photo, the Sun is forward and to the upper right with a solar elevation of approximately 48°; because of this, the glare spot seen is almost certainly due to reflection of light from the droplet and not from refraction. Further confirmation of this is the fact that the glare spot in Fig. 1 shows no dispersion of colors, and the separation of colors in the interference fringe in Fig. 2 is very slight and characteristic of diffraction (i.e., longer wavelengths to larger angles) rather than dispersion, which would separate the colors more and which would refract shorter wavelengths to higher angles. In Fig. 1, the glare spot seems to be
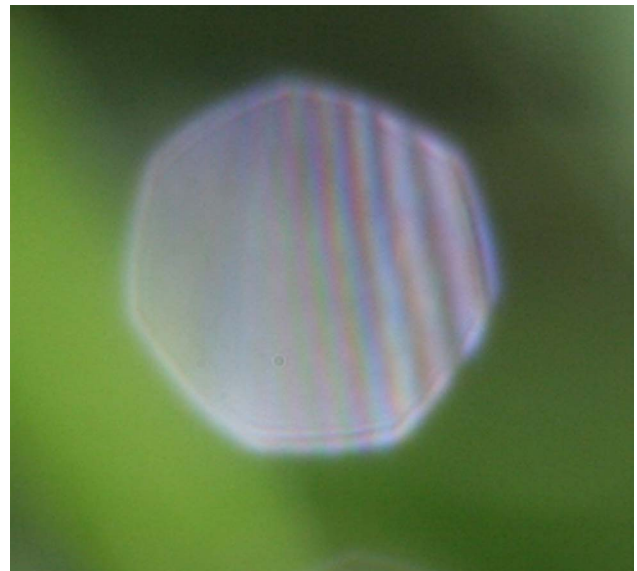

Fig. 2. (Color online) Out-of-focus image of the glare spot from Fig. 1 showing Airy fringes.

near a point of inflection in the droplet shape, occurring as it does very near the point of attachment of the droplet to the blade of grass; however, this cannot be seen directly, as the glare spot obscures the shape of the droplet at that point.

In the rest of this paper we develop a theory to characterize the external reflection rainbow caustic from a pendant droplet when the incident beam is perfectly horizontal. We then compare the results of the theory developed to several qualitative experiments done on pendant droplets. In a companion paper [6] we examine the case of arbitrary incidence theoretically and then compare the results of that theory with observations of naturally occurring external reflection rainbows. In that paper we also discuss the application of this work to fluids diagnostics.

2. Theory

A. Geometry of the Pendant Droplet

Consider a water droplet hanging from either a leaf or a thin straight vertical wire. The pendant droplet is assumed to be rotationally symmetric about the vertical axis, which is taken to be the z axis of an xyz coordinate system. The nonlinear differential equation that describes its shape has long been known, and numerical solutions are available for droplets with differing radii of curvature at the bottom [7]. The shape of a pendant droplet resembles a prolate spheroid attached by a narrow neck to the leaf or thin straight wire. Just below the neck region, the droplet surface possesses an inflection point, which when rotated around the droplet is what we hereafter call the inflection circle. The inflection circle has radius r_i and is a height z_i above the origin of the coordinates. The first three terms in the Taylor series expansion of the surface shape in the vicinity of the inflection circle are

Fig. 1. (Color online) Droplet with reflected glare spot. Note that the glare spot appears where the droplet curvature goes from convex to concave.

$$r(z) = r_i - (z - z_i)\tan(\xi) + \alpha(z - z_i)^3, \qquad (1)$$

where α is presumably small. At $z = z_i$ the droplet surface is tangent to a cone with opening half-angle ξ. The $\alpha(z - z_i)^3$ term in Eq. (1) models the beginning of the narrowing of the neck of the droplet outside the tangent cone for $z > z_i$ and the beginning of the rounded body of the droplet inside the tangent cone for $z < z_i$. Figure 3 shows a surface plot of the pendant droplet in the region near the circle of attachment to its support. We found it easier to use Eq. (2) below to generate the image; the values of the parameters used to create the image are the tangent cone angle, $\xi = \pi/6$ (=30°); the radius of the circle of attachment, $r_{att} = 0.1$ (in arbitrary units); the radius of the inflection circle, $r_0 = 0.8$; the cubic coefficient, $\alpha/\tan^4(\xi) = 0.75$. These do not match any data shown below, but were simply chosen to best highlight the shape of the droplet near the inflection circle. Figure 3 also includes arrows defining the directions of the incident and reflected rays, plus the angles ϕ, φ and θ defined below in the paper.

If the radius of curvature of the bottom of the droplet is relatively large, as is the case for $\beta \approx 0.5$ in Table 3B and Fig. 10 of [7], where the droplet was assumed to hang from a flat wet horizontal surface, the cubic form of Eq. (1) remains an accurate approximation to the surface shape all the way from the narrowest part of the neck of the droplet to the widest part of the body. But for the case of a droplet hanging from a leaf or a thin wire, which perhaps corresponds closer to $\beta \approx 0.2$ in Fig. 10 of [7], the narrowest part of the neck and the widest part of the body are quite asymmetric. Thus many more terms in the Taylor series expansion of $r(z)$ are required in order to accurately approximate the surface shape of the pendant droplet all the way from the narrowest part of the neck to the widest part of the body. But even in these situations, Eq. (1) remains an accurate approximation to the surface shape as long as points sufficiently close to the inflection circle are considered. Equation (1) can be approximately inverted to give

$$z(r) = z_i - (r - r_i)/\tan(\xi) - \alpha(r - r_i)^3/\tan^4(\xi) \qquad (2)$$

as long as $3\alpha(r - r_i)^2/\tan^3(\xi) \ll 1$. If the angle in the horizontal plane with respect to the $+x$ axis in cylindrical coordinates is θ, the outward unit normal to the droplet surface is

$$\mathbf{n} = \{-(\partial z/\partial r)[\cos(\theta)\mathbf{u_x} + \sin(\theta)\mathbf{u_y}] + \mathbf{u_z}\}$$
$$/[(\partial z/\partial r)^2 + 1]^{1/2}. \qquad (3)$$

B. Geometry of the Incident Beam

Consider a family of parallel light rays of wavelength λ incident on the droplet in the vicinity of the inflection circle. We define a coordinate system (x, y, z) in relation to the central vertical axis of the droplet such that z is the vertical axis (and is also the symmetry axis of the droplet), the beam is incident in the xz plane, propagating in the $+x$ direction, and the direction of the y axis is defined in terms of the standard right-handed coordinate system. Figures 3 and 4 have the relevant angles for the incident and scattered rays labeled. In Figure 3, the out-of-plane scattering is shown, including the angles that the incident and scattered rays make with the xy plane (ψ and ϕ, respectively.) Figure 4 shows a slice of the coordinate system in the xy plane (i.e., as viewed from a vantage point directly above the droplet, along the $+z$ axis). The incoming ray is moving in the direction of the $+x$ axis (which is drawn vertically on the page.) It intersects the droplet at a radial distance $r(z)$ (=r) from the z axis. Drawing a horizontal line from the symmetry axis to the intersection point, the angle that the line makes with the $+y$ axis is ε. If we now examine the scattered ray, the angle that the scattered ray makes with the $+x$ axis is θ. Note that if the rays is unscattered $\varepsilon = \theta$. The coordinate $z = 0$ marks the point of inflection of the droplet. We define the impact parameter $b = r \cos(\varepsilon)$ as the distance from the z axis at which the incident ray intersects the droplet.

The wave vector of a ray in the family is

$$\mathbf{k_{inc}} = \cos(\psi)\mathbf{u_x} - \sin(\psi)\mathbf{u_z}. \qquad (4)$$

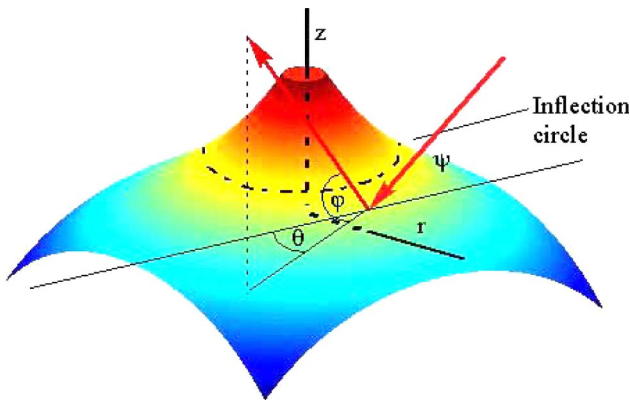Fig. 3. (Color online) Shape of the droplet near the circle of attachment to its support. $\xi = p/6$ (30°), $\alpha/\tan^4(\xi) = 0.75$, $r_{att} = 0.1$, $r_0 = 0.8$.
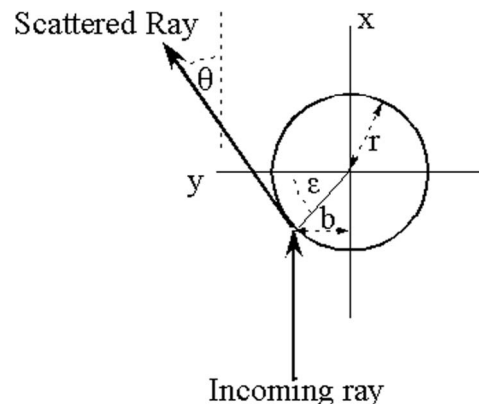

Fig. 4. Top view of the coordinate system used in this paper.

If $\psi = 0$ the rays are said to be horizontally incident on the droplet, and if $\psi \neq 0$ they are said to be diagonally incident. If an incident ray grazes the surface of the droplet and is reflected, it is called a grazing incident ray. If it is reflected from any other portion of the droplet, it is called a ray with arbitrary incidence.

The family of incident rays that reflect from the pendant droplet in the vicinity of the inflection circle form an Airy caustic or rainbow in the far zone. In this paper we consider the cases of grazing horizontal incidence and arbitrary horizontal incidence separately, as there are a number of simplifications that one can make in the first case, while additional features of the Airy caustic appear in the theoretically more complicated second case. In the companion paper [6] we consider the case of diagonal incidence.

C. Grazing Horizontal Incidence

Consider a family of light rays traveling parallel to the x axis with $\psi = 0$ that are incident on the droplet in the vicinity of the inflection circle. A given ray in the family strikes the droplet surface with the angle ε in the horizontal plane, where $0 \leq \varepsilon \leq \pi$, and at the height $z = z_i + \delta$ above the xy plane. The unit vector in the incident direction is

$$\mathbf{k_{inc}} = \mathbf{u_x}. \tag{5}$$

Near-grazing-incident rays are characterized by $\sin(\varepsilon) \approx \varepsilon$ and $\cos(\varepsilon) \approx 1$. The direction of the reflected rays is given by

$$\mathbf{k_{ref}} = \mathbf{k_{inc}} - 2(\mathbf{k_{inc}} \cdot \mathbf{n})\mathbf{n}. \tag{6}$$

Near-grazing-incident rays are reflected in the near-forward direction. Note that the reflection angles θ and ϕ are defined with respect to a standard spherical coordinate system in which ϕ represents the polar angle (really, the complement of the polar angle) with respect to the z axis and θ is the angle that the projection of the ray into the xy plane makes with the $+x$ axis. We need now to reference the rays to a rotated coordinate system more suitable for examining the scattered light; in this coordinate system, Θ represents the angle that the scattered ray makes with the $+x$ axis, while Φ represents the angle that the projection of the ray into the yz plane makes with the $+z$ axis. The two sets of angles are shown in Fig. 5. In this coordinate system,

$$\tan(\Phi) = (k_{ref})_z/(k_{ref})_y, \tag{7}$$

$$\Theta \approx \tan(\Theta) = [(k_{ref})_y{}^2 + (k_{ref})_z{}^2]^{1/2}/(k_{ref})_x. \tag{8}$$

Substituting Eqs. (2), (3), and (5) into Eq. (6), and the result into Eqs. (7) and (8), we obtain
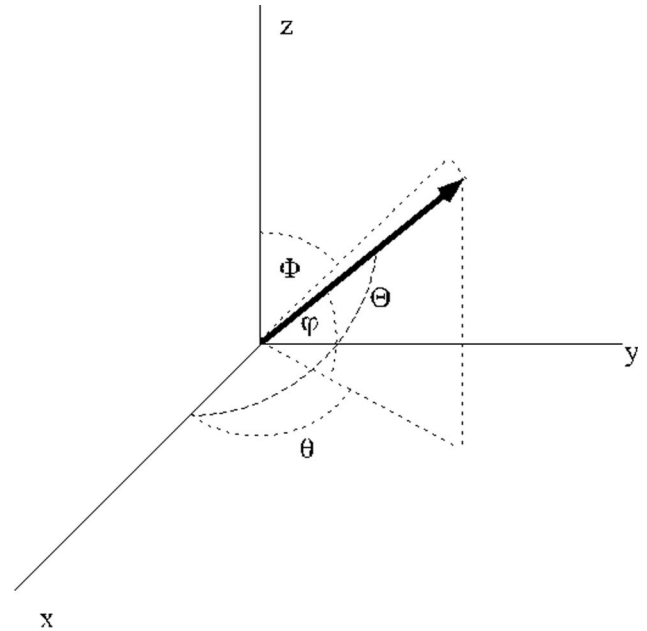
$$\tan(\Phi) = \tan(\xi) - 3\alpha\delta^2, \tag{9}$$

Fig. 5. Coordinate system showing the definitions of the two sets of scattering angles (θ, ϕ) and (Θ, Φ) used in this paper.

$$\Theta = 2\varepsilon \cos(\xi). \tag{10}$$

In obtaining this result we assumed that the rays are close enough to the inflection circle that $\alpha\delta^2 \ll 1$ and that terms in the direction of the reflected ray of order α^2 can be neglected.

Equations (9) and (10) demonstrate that two incident rays striking the droplet at the same angle ε but at different heights $z = z_i \pm \delta$ are both reflected in the same direction and thus interfere in the far zone. In the limit $\varepsilon \to 0$, $\Phi \to \xi$, this corresponds to grazing incident rays striking the inflection circle near $\delta = 0$, marking the boundary between the region below the $\Phi = \xi$ line illuminated at each point by two rays and the nonilluminated region above it. In wave theory, this two-ray to zero-ray transition is the Airy caustic. The reflection geometry considered here satisfies the general condition for the existence of a far-zone reflection caustic. When a plane wave is reflected by a surface of arbitrary shape, the reflected intensity at any scattering angle is proportional to the product of the principal radii of curvature of the surface at the corresponding point on the surface from which the ray reflects [8]. For the pendant droplet geometry, the radius of curvature of the droplet surface in the vertical plane is infinite on the inflection circle, leading to an infinite scattered intensity in ray theory, which becomes softened to a large but finite intensity on the caustic in wave theory. In the limit $\varepsilon \to 0$ (corresponding to near-grazing incidence) the shape of the rainbow on a far-zone viewing screen a distance R from the droplet and normal to the positive x axis is the straight line $\Phi = \xi$. As ε increases for incident rays with $\delta = 0$, the scattering angle Θ of the rainbow

on the viewing screen also increases. It should be noted that when the small-angle approximation is no longer valid, the shape of the rainbow on the viewing screen becomes curved. This will be discussed in detail in Subsection 2.D.

For scattering of a plane wave by a homogeneous sphere, one usually obtains the argument of the Airy caustic for the $p - 1$ internal reflection rainbow by propagating an initially flat wavefront through the sphere in the vicinity of the Descartes ray and obtaining the wavefront in the exit plane. The exiting wavefront is quadratic in one direction and cubic in the other direction. The exit plane wavefront is then Fraunhofer diffracted to the far zone, yielding the Airy caustic [9]. Since the limit of the Airy caustic far into the lit region is the interference of two parallel supernumerary rays [9], we use the alternative procedure of first determining the path length difference of the two supernumerary rays and then working backward to infer the argument of the Airy caustic.

First consider light rays reflected at near-grazing incidence from a cone with opening half-angle ξ [i.e., $\alpha = 0$ in Eqs. (1) and (2)]. Recall that this cone is tangent to the surface of the pendant droplet at the inflection circle. All reflected rays having the same angle of incidence ε but with differing incident heights $z = z_i + \delta$ are reflected in exactly the same direction in the far zone, $\Phi = \xi$. They also have exactly the same path length from the cone's entrance plane to its exit plane. These rays constructively interfere in the far zone, producing an infinite intensity in ray theory. The addition of the perturbation $\alpha(z - z_i)^3$ to the surface shape in Eq. (1) serves to deflect rays with different values of $|\delta|$ into different directions. It also changes the path length of the $+\delta$ ray from that of the $-\delta$ ray, thus weakening the intensity at $\Phi = \xi$ to that of the rainbow peak. Ignoring terms of order ε^2 and α^2, the path length of the ε, $z_i + \delta$ incident ray is longer than that of the ε, $z_i - \delta$ ray by

$$\Delta s_{\text{incoming}} = 2\varepsilon\delta[\tan(\xi) - \alpha\delta^2], \qquad (11)$$

and the path length of the reflected rays differs by

$$\Delta s_{\text{outgoing}} = -2\varepsilon\delta[\tan(\xi) - \alpha\delta^2] + 8\varepsilon\alpha\delta^3 \cos^2(\xi), \quad (12)$$

giving a total phase difference of

$$\Delta\varphi = k(\Delta s_{\text{incoming}} + \Delta s_{\text{outgoing}}) = 8k\varepsilon\alpha\delta^3 \cos^2(\xi), \qquad (13)$$

where $k = 2\pi/\lambda$. The total normalized electric field of the two interfering rays is then proportional to

$$E_{\text{total}}(\varepsilon, \delta) \approx \cos(\Delta\varphi/2 - \pi/4)$$
$$= \cos\{4k\varepsilon\alpha\delta^3\cos^2(\xi) - \pi/4\}, \qquad (14)$$

where it is assumed that, as is the case for the $p - 1$ internal reflection rainbow of a homogeneous sphere,

one of the two participating supernumerary rays crosses a near-zone focal line and acquires an additional phase shift of $\pi/2$.

Equation (14) is inconvenient in the sense that the total field is written in terms of the incoming ray parameters ε and δ rather than in terms of the angles Θ and Φ observed on the far-zone viewing screen. If Φ is written as

$$\Phi = \xi - \Gamma \qquad (15)$$

with $\Gamma \ll 1$, substituting Eq. (15) into Eq. (9) gives

$$\Gamma \approx 3\alpha\delta^2 \cos^2(\xi). \qquad (16)$$

On the far-zone viewing screen, the radial distance ρ along the rainbow line $\Phi = \xi$ from the point where the positive x axis crosses the viewing screen is

$$\rho = R\Theta, \qquad (17)$$

and the tangential distance σ on the viewing screen that cuts across the supernumerary interference pattern is

$$\sigma = R\Theta\Gamma. \qquad (18)$$

Substitution of Eqs. (10) and (16)–(18) into Eq. (14) gives

$$E_{\text{total}}(\rho, \sigma) \approx \cos\{2k\sigma^{3/2}/[3^{3/2}\alpha^{1/2}\rho^{1/2}R \cos^2(\xi)] - \pi/4\}. \qquad (19)$$

Making the association in the $w \to \infty$ limit [10]

$$\text{Ai}(-w) \approx \cos(2w^{3/2}/3 - \pi/4), \qquad (20)$$

we obtain

$$E_{\text{total}}(\rho, \sigma) \approx \text{Ai}\{-k^{2/3}\sigma/[3^{1/3}\alpha^{1/3}R^{2/3}\rho^{1/3}\cos^{4/3}(\xi)]\} \qquad (21)$$

as the rainbow produced by rays with near-grazing horizontal incidence in the vicinity of the inflection circle of a pendant droplet. The constant of proportionality multiplying the Airy integral of Eq. (21) will be derived in Subsection 2.D.

The horizontal grazing incidence geometry considered above is sufficiently uncomplicated that the shape of the wavefront in the exit plane can be straightforwardly determined and then Fraunhofer diffracted to the far zone. This check of the procedure leading to Eq. (21) is performed to justify the supernumerary path length difference procedure so that it can be applied to the more complicated case of diagonal incidence to be considered in [6]. (i) The entrance and exit planes were chosen to be perpendicular to the incoming and outgoing rainbow ray with the input parameters ε and $\delta = 0$, and contained the point where the ray strikes the droplet surface.

Another ray with the same value of ε but with $\delta \neq 0$ was also considered, and its path length was calculated between the entrance and exit planes. It should be noted that although the trajectories of the rainbow ray and the $\varepsilon, \delta \neq 0$ rays are parallel on the incoming side of the reflection, they are not parallel on the outgoing side. The path length difference between the two rays was found after much algebra to be

$$\Delta s_{\text{total}} = 2\alpha\varepsilon\delta^3 \cos^2(\xi). \qquad (22)$$

(ii) Again this path length must be expressed in terms of exit plane variables instead of entrance plane variables. Let $\mathbf{u}$ be the vector in the exit plane from the point where the rainbow ray crosses the exit plane to the point where the $\varepsilon, \delta \neq 0$ ray crosses it. The length of $\mathbf{u}$ was calculated to be

$$u = \delta / \cos(\xi), \qquad (23)$$

and the phase difference of the $\delta = 0$ and $\delta \neq 0$ rays in the exit plane is

$$\Delta\varphi = k\alpha\Theta u^3 \cos^4(\xi). \qquad (24)$$

(iii) This exit plane wavefront is then Fraunhofer diffracted an angle $\gamma = \Gamma\Theta$ below the $\mathbf{k_{ref}}$ direction in the plane formed by $\mathbf{k_{ref}}$ and $\mathbf{u}$. The result is identical to Eq. (21).

D. Arbitrary Horizontal Incidence

In both this subsection and the next, we determine the trajectory and intensity along the Airy caustic produced by reflection of a family of parallel incident rays from a pendant droplet that range from grazing incidence to head-on incidence. Since the surface of the pendant droplet is tangent to a cone of opening half-angle ξ at the inflection circle, these results are equivalent to those for reflection of the rays from the cone. We consider the case of horizontal incidence with $\psi = 0$ and $0 \leq \varepsilon \leq \pi/2$. We parameterize a ray on the wavefront by its horizontal distance b' from the $-x$ axis and its height z' above the xy plane. We surround the cone with a cylindrical viewing screen of radius $R \to \infty$ whose axis coincides with the axis of the cone. The scattering angles of a reflected ray on the cylindrical viewing screen are taken to be θ with respect to the $+x$ axis in the horizontal plane and ϕ above the horizontal plane.

Defining the parameter Ω by

$$\Omega = \sin(\varepsilon) \cos(\xi), \qquad (25)$$

the set of incident rays with constant z' and with b' ranging from grazing incidence to head-on incidence corresponds to

$$0 \leq \Omega \leq \cos(\xi). \qquad (26)$$

Substituting Eqs. (5) and (25) and the definitions of θ and ϕ into Eq. (6), the scattering angles of the rays

reflected from the cone are

$$\sin(\phi) = 2\Omega \sin(\xi), \qquad (27)$$

$$\cos(\theta) = (1 - 2\Omega^2)/[1 - 4\Omega^2 \sin^2(\xi)]^{1/2}. \qquad (28)$$

The trajectory of the Descartes ray of the Airy caustic on the cylindrical viewing screen is

$$\begin{array}{ll} 0 \leq \phi \leq 2\xi & \text{if } \xi \leq \pi/4, \\ 0 \leq \phi \leq \pi - 2\xi & \text{if } \xi \geq \pi/4, \end{array} \qquad (29)$$

$$\begin{array}{ll} 0 \leq \theta \leq \pi & \text{if } \xi < \pi/4, \\ 0 \leq \theta \leq \pi/2 & \text{if } \xi = \pi/4, \\ 0 \leq \theta \leq \theta_{\max} & \text{if } \xi > \pi/4, \end{array} \qquad (30)$$

where

$$\cos(\theta_{\max}) = [1 - 2\cos^2(\xi)]^{1/2} / \sin^2(\xi). \qquad (31)$$

Figure 6 shows plots of the trajectory of the principal peak of the caustic for different values of the tangent cone angle. We plot the variables $1 - \cos(\theta)$ on the horizontal axis and $\tan(\phi)$ on the vertical to facilitate comparison with experimental results presented below. The reason we use these somewhat unusual coordinates is as follows: in the experiments described below, light was scattered from a pendant droplet onto a cylindrical screen concentric with the droplet, and the pattern was photographed from a relatively large distance away. The center of the screen corresponds to a scattering angle $\theta = \pi/2$, or $\varepsilon = 0$; however, the photograph is essentially a projection of the scattering pattern onto a flat screen. Because of this, the horizontal coordinate in the photograph is given by $1 - \cos(\theta)$. Similarly, the vertical coordinate is proportional to $\tan(\phi)$. Using these coordinates makes comparison with experimental results direct.

As b' is varied from grazing incidence to head-on incidence for constant z', the angle θ of the principal peak of the Airy caustic either increases monotonically from zero (i.e., forward scattering) to π when $\xi < \pi/4$, or from zero to $\theta_{\max}$ when $\Omega = 1/[2^{1/2} \tan(\xi)]$ and then decreases back from $\theta_{\max}$ to zero when $\xi > \pi/4$ as the other scattering angle ϕ monotonically increases from zero to some value less than or equal to $\pi/2$. Since $d\theta/d\phi = 0$ at $\theta_{\max}$, the trajectory of the Airy caustic is smooth at the turnaround point in θ, and a higher-order caustic such as a cusp does not occur there.

As mentioned in Subsection 2.C, if the principal radii of curvature of the reflecting surface are both finite, the intensity of the reflected light in ray theory is related in a simple way to the Gaussian curvature at the point on the surface that is mapped into the direction of the reflected ray. But for a reflecting cone, the radius of curvature of its surface in the vertical
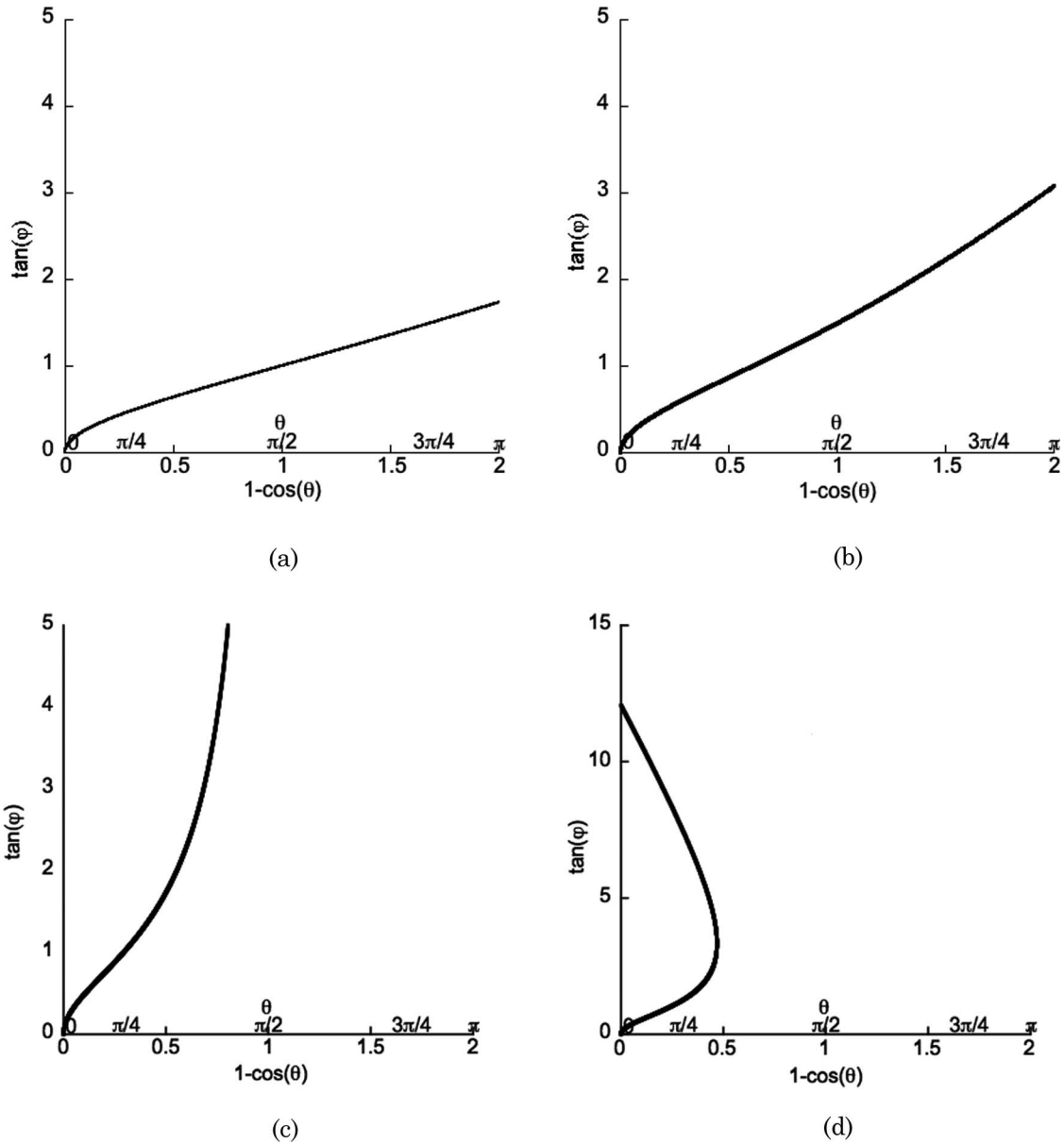
Fig. 6. Shape of external reflection rainbow caustic scattered onto a cylinder centered on the droplet. (a) $\xi = \pi/6$ (30°), (b) $\xi = \pi/5$ (36°), (c) $\xi = \pi/4$ (45°), (d) $\xi = \pi/3.8$ (47.4°).

plane is infinite. Thus, the usual method of obtaining the reflected intensity is inapplicable, and another approach must be taken. The approach we used to determine the intensity of light reflected by a cone consists of the following three steps. (i) Consider a ray on the incident wavefront parameterized by (b', z'). Determine the point (x_0, y_0, z_0) where the ray strikes the cone surface, and the point

$$\mathbf{R} = x_{\mathrm{vs}}\mathbf{u_x} + y_{\mathrm{vs}}\mathbf{u_y} + z_{\mathrm{vs}}\mathbf{u_z}, \qquad (32)$$

where the reflected ray intercepts the far-zone cylindrical viewing screen. (ii) With z' constant, vary the incident ray from b' to $b' + \mathrm{d}b'$ and determine the new position of the reflected ray $\mathbf{R}'$ on the viewing screen

$$\mathbf{R}' = \mathbf{R} + \mathbf{dR}' = \mathbf{R} + (\partial \mathbf{R}/\partial b')\mathrm{d}b'. \qquad (33)$$

(iii) With b' constant, vary the incident ray from $z\prime$ to $z' + \mathrm{d}z'$ and determine the new position of the reflected ray $\mathbf{R}''$ on the viewing screen

$$\mathbf{R}'' = \mathbf{R} + \mathbf{dR}'' = \mathbf{R} + (\partial \mathbf{R}/\partial z')\mathrm{d}z'. \qquad (34)$$

(iv) The area of the incident flux tube subtended by these rays is $\mathrm{d}b'\mathrm{d}z'$, and the area of the reflected flux tube on the viewing screen is $|\mathbf{dR}' \times \mathbf{dR}''|$. Thus, if the incident ray intensity is I_{inc}, the reflected ray intensity on the viewing screen is, by conservation of energy,

$$I_{\mathrm{ref}} = I_{\mathrm{inc}}/[|(\partial\mathbf{R}/\partial b') \times (\partial\mathbf{R}/\partial z')|\cos(\phi)], \qquad (35)$$

assuming the cone to be perfectly reflecting. (In this paper we use the common physics parlance "intensity" to refer to incident power/unit area rather than the more correct photometric term "radiometric irradiance," as the former term is more commonly used than the latter.) Applying this procedure to a family of rays horizontally incident on a reflecting cone, we obtain after much algebra

$$I_{\text{ref}} = I_{\text{inc}} r_0 \, \sin(\phi) \cos(\phi) / \{R \, \tan(\xi)[4\cos^2(\xi) - \sin^2(\phi)]\}, \tag{36}$$

where r_0 is the radius of the cone cross section in the horizontal plane of constant z'. The advantage of writing Eq. (36) as a function of ϕ is that experimentally one observes the trajectory of the Airy caustic as a function of θ and ϕ on the viewing screen. Then for an observed value of ϕ, one can measure the intensity of the caustic and straightforwardly compare the result to Eq. (36). If one wished to instead express Eq. (35) as a function of the input ray parameters b' and z' or, equivalently, in terms of ε, where

$$\cos(\varepsilon) = b'/r_0, \tag{37}$$

Eq. (36) becomes

$$\begin{aligned} I_{\text{ref}} = I_{\text{inc}} \, \sin(\varepsilon)(r_0/R)[\cos^2(\varepsilon) \\ + \sin^2(\varepsilon)\cos^2(2\xi)]^{1/2}/\{[1+\cos(2\xi)] \\ + \cos^2(\varepsilon)[1-\cos(2\xi)]\}. \end{aligned} \tag{38}$$

3. External-Reflection Rainbow Caustics in the Laboratory

In this section we discuss the creation of an external-reflection rainbow using pendant droplets in a laboratory setting. To examine the caustics, we took a syringe filled with water with a needle whose point was ground flat; the radius of the needle is 0.5 mm. By pressing the plunger gently we could create droplets similar to those seen in Fig. 1, but whose size could be varied. We expected that the smaller the droplet, the larger the cone angle ξ, as the shape of the droplet is determined by the competition between surface tension and weight; the greater the weight, the more the droplet will be distended. This was in fact seen to be the case.

To view the caustic, we shined a beam from a He–Ne laser (wavelength $\lambda = 632.8$ nm) onto the pendant droplet near the inflection circle. (The wavelength corresponds to the red region of the spectrum; however, in some images the scattered light appears bluish white because of camera saturation.) To view the section of the caustic due to near-grazing-incidence rays, we placed a screen (a piece of paper) forward of the droplet so that light scattered in the near-zero angle direction could be seen. Figure 7 is a diagram of our experimental setup. We photographed the caustic using a $50 webcam (resolution 640×480 pixels); to make it useful, we removed the camera board from its case, so that the camera lens could be unscrewed almost completely from its mount to get close-up photographs. We found that the image quality was excellent despite the low cost of the system.

Figure 8 is a picture of the pendant droplet; Fig. 9 shows the external reflection caustic from that droplet. Figure 10 shows a close-up of a section of the caustic of Fig. 9; in this image, Airy fringes are clearly seen, showing that this is a fold caustic. The fringes are perpendicular to the caustic line, again as predicted by theory. Note that, from Eq. (21), the spacing of the Airy fringes should increase with ρ, which is what we observe, although we have not made any attempt to make a quantitative match with theory.

To see the caustic due to all of the rays, not just the ones at near-grazing incidence, we placed a cylindrical screen centered on the droplet (see Fig. 4); this enabled us to examine the caustic structure from scattering angles of near 0° (forward) to near 180° (i.e., backward.) One prediction that theory makes is that for a droplet whose tangent cone angle is greater than 45° there will be no light scattered backward [see Eqs. (27)–(31) and Figs. 6(c) and 6(d)]. To verify this, we examined the caustics for three droplets of increasing size; Fig. 11(a) shows the smallest droplet, while Fig. 11(b) shows the caustic produced by it. Unfortunately, the smallest droplets produced by this syringe were highly asymmetric, which makes a quantitative fit to the theory impossible, but it is clear that the caustic curves backward at large angles. Even though the droplet is highly asymmetric, the global behavior of the caustic is very similar to that predicted by theory, and we can safely regard the theory as an approximation to true behavior.
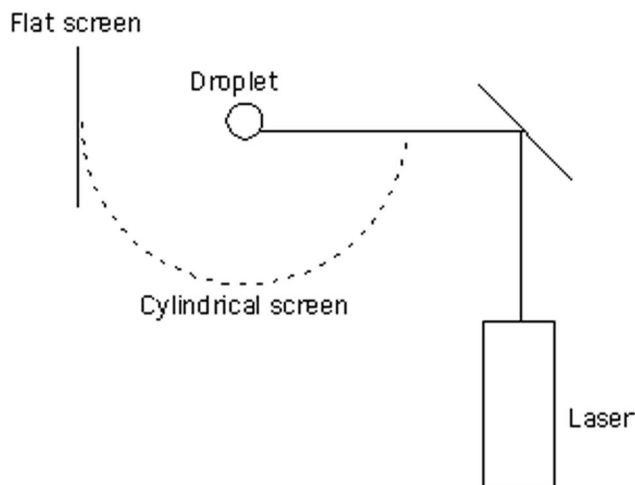

Fig. 7. Experimental apparatus for photographing external reflection caustics in the laboratory. The flat viewing screen was used for looking at caustics in the near-0° scattering direction; the semicylindrical screen was used to examine the caustics from 0° to 180°.

Fig. 8. (Color online) Photograph of pendant droplet. The image has been cropped slightly. The droplet is viewed from the forward (i.e, $\theta = 0$) direction; the laser beam creating the caustic will be reflected from the droplet at its upper right.

Fig. 10. (Color online) Magnified image of section of the caustic from Fig. 7. Airy fringes are clearly visible near the caustic.

Figure 12(a) shows a medium-sized droplet, and Fig. 12(b) the caustic produced by it. In this case, the tangent cone angle at the inflection circle seems to be around 45°, as the caustic seems to be at the borderline case where the caustic extends only to $\theta = \pi/2$. Figure 13(a) shows the largest droplet that can be produced by the syringe before the drop fissions off, and Fig. 13(b) shows the caustic due to it; as can be seen, the caustic structure extends to scattering angles of 180°, consistent with the smaller tangent cone angle for the larger droplet. Comparison of Figs. 11(b), 12(b), and 13(b) should be made to Figs. 6(a)–6(d); the qualitative agreement between the two sets of figures is striking, although there are differences that we believe are due to the fact that the droplets produced in the laboratory (especially the smallest ones) are not radially symmetric.
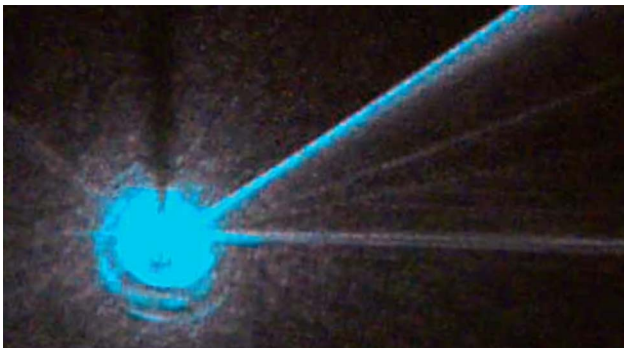

(a)

(b)

Fig. 11. (Color online) (a) Photograph of small pendant droplet. The droplet is obviously asymmetric. (b) External reflection caustic produced by droplet in (a). Comparison to Fig. 6(d) is of interest.

Fig. 9. (Color online) External reflection rainbow caustic, near-0° scattering angle. The horizontal line seen in the lower half of the figure is due to reflection from the needle.
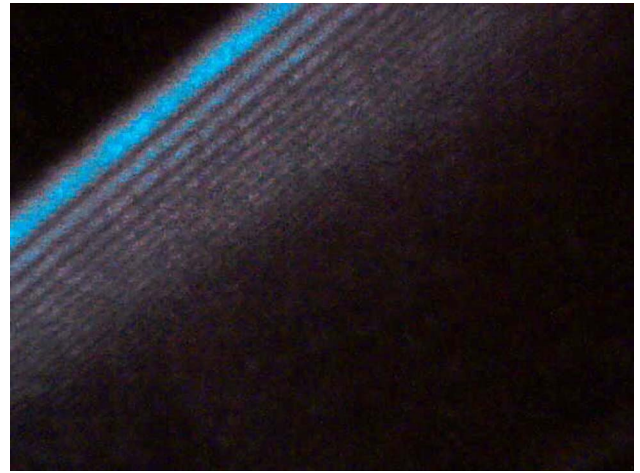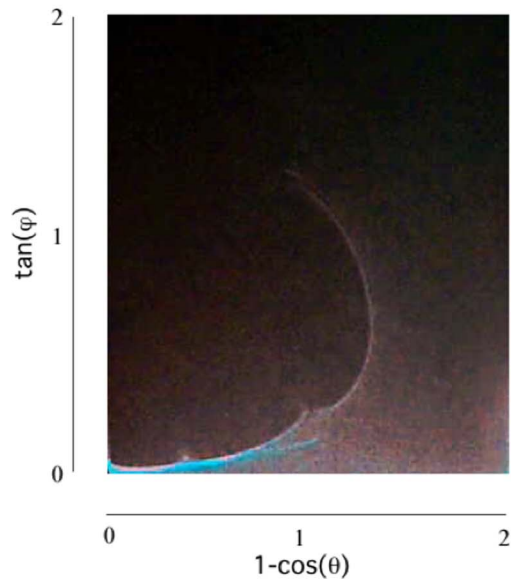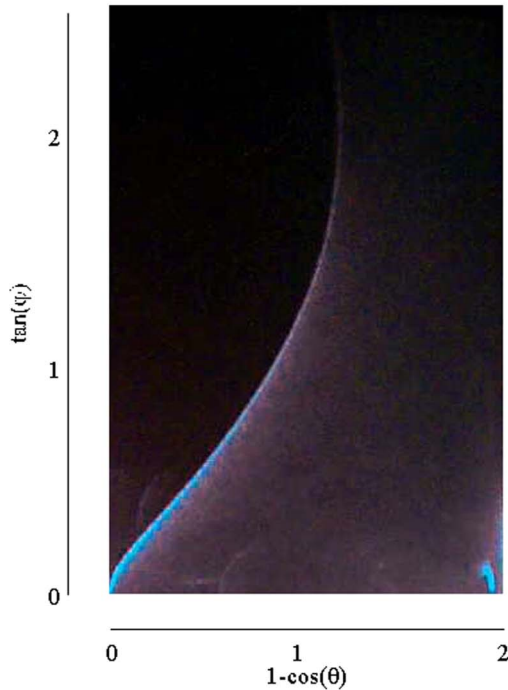
(a)

(b)

Fig. 12. (Color online) (a) Photograph of intermediate size pendant droplet. (b) External reflection caustic produced by droplet in (a). Comparison to Fig. 6(c) is of interest.

(a)

(b)

Fig. 13. (Color online) (a) Photograph of large droplet; the droplet is not much larger than that in Fig. 12(a), but the behavior of the caustic is strikingly different. (b) External reflection caustic produced by droplet in (a).
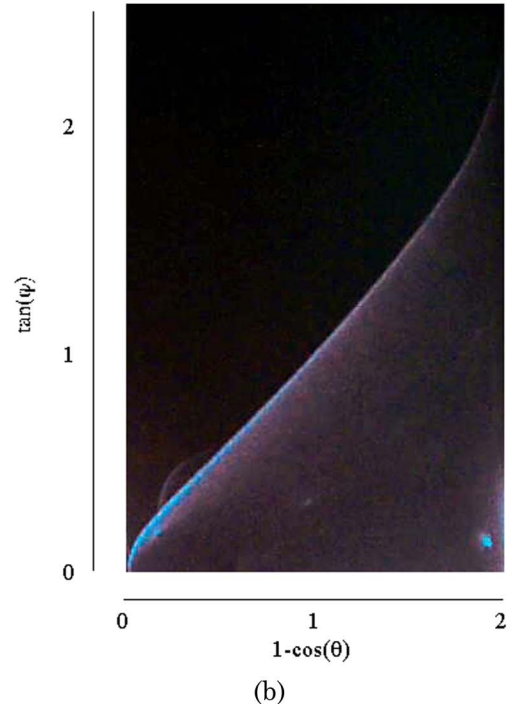
In particular, in Fig. 9, the caustic clearly extends to scattering angles greater than $\pi/2$ before folding back to smaller scattering angles; we expect the deviations of the caustic structure created by this droplet from theory to be large, however, as the droplet is so asymmetric.

4. Conclusions

We have examined the external reflection rainbow caustic produced by a pendant water droplet where the incident light beam is horizontal and the droplet is radially symmetric in the horizontal plane. We show good qualitative agreement between theory and laboratory experiment; however, to extend the comparison to observation, we must extend the theory to account for arbitrary angle of incidence; this is accomplished in the companion paper [6] dealing with this topic in the Feature issue.

References

1. O. N. Stavroudis, *The Optics of Rays, Wavefronts and Caustics* (Academic, 1972), p. 79.
2. See, for example, R. Greenler, *Rainbows, Halos and Glories* (Cambridge U. Press, 1980), pp. 1–7.
3. H. C. van de Hulst, *Light Scattering by Small Particles* (Dover, 1981), pp. 240–246.
4. C. L. Adler, V. A. Smith, and N. M. Haddad, "Rainbow surface tension analysis," Opt. Express **16**, 5118–5129 (2008).

5. L. H. Tanner, "The surface tension effect on the flow of liquid down vertical or inclined surfaces," J. Phys. D **13**, 1633–1641 (1980).

6. J. A. Lock, R. W. Fleet, and C. L. Adler, "Rainbows in the grass. II. Arbitrary diagonal incidence," Appl. Opt. 47, H214–H219 (2008).

7. J. F. Padday, "The profiles of axially symmetric menisci," Philos. Trans. R. Soc. London Ser. A **269**, 265–293 (1971).

8. P. L. Marston, "Geometrical and catastrophe optics methods in scattering," Phys. Acoust. **21**, 1–234 (1992), Eq. (57).

9. W. J. Humphreys, *Physics of the Air* (Dover, 1964), pp. 484–492.

10. M. Abramowitz and I. A. Stegun, eds., *Handbook of Mathematical Functions* (National Bureau of Standards, 1964), p. 448, Eq. (10.4.60).